Special Feature: Drivetrain and Braking Technology

Research Report

Structural Design Technology for Brake Squeal Reduction: Technology for Measuring the Distribution of Friction Force and Optimizing Contact Surface

Yoshitsugu Goto, Yuji Nagasawa and Toru Matsushima

∎**ABSTRACT**∥ The contact condition of friction surfaces has a significant influence on brake squeal. However, technology has yet to be developed that is capable of measuring the dynamic force distribution of friction surfaces. Therefore, in the present study, we examine technology for measuring the distribution of normal pressure and friction forces between the brake disk rotor and the brake pads under braking conditions. Since friction parts, such as brake pads, are the subject of the present study, sensors are built into a brake disk rotor to be used in the experiments. The present paper outlines the structure of a prototype sensor and describes several experimental measurements. The force distribution is shown for various combinations of caliper alignment, rotor temperature, and brake torque. Moreover, we demonstrate that the finite element method (FEM) is effective for analyzing brake squeal phenomena. Although FEM analysis can be used to easily obtain squeal frequencies and complex vibration modes, it is difficult to identify how to modify the contact conditions between components. Therefore, in the present study, we propose a practical design method to reduce brake squeal that is capable of optimizing the contact conditions through sensitivity analysis.

∎**KEYWORDS**∥ Brake, Squeal, Noise, Vibration, Sensor, Measurement, Friction, FEM, Simulation, Stiffness

1. Introduction

The contact condition of a friction surface has a great influence on brake squeal and noise.[1-3] In order to measure the distribution of normal force, pressure sensitive sensors[4] or tactile sensors[5] are usually inserted between the disk rotor (hereinafter, rotor) and pads. The pressure distribution is easily measured using such commercial products. However, these products are not available under braking conditions. Therefore, in the case of using such products, the pressure distribution under braking conditions is predicted from the pressure distribution under the stopped state.

On the other hand, several measurement methods[6,7] have been proposed in order to directly measure the contact condition under braking conditions. However, the mechanical and thermodynamic conditions in the actual brake system are difficult to reproduce using dedicated test equipment. Moreover, in the case of inserting load cells into pads,[8] the harmful influence of processing pads for measurement cannot be ignored.

In order to address these issues, the present study investigates how to equip a running rotor with appropriate load cells. The present article proposes a sensor structure and a measurement method and reports the effectiveness of the proposed technology through a number of application examples.

In the latter half of this article, a brake squeal simulation is conducted, and an optimization technology is proposed. Stability analysis of point mass systems[9] was performed in the 1970s, and the use of complex eigenvalue analysis using the finite element method (FEM) increased in the 1990s. The FEM is capable of reflecting design geometry in detailed analysis results, and so is, at present, widely used in product development. However, even if FEM analysis is used to obtain the frequency and vibration mode of squeal, FEM analysis is insufficient for identifying a specific design policy.[10] As a countermeasure to reduce brake squeal, several methods have been considered for optimizing contact conditions between parts. This article describes the difficulty in reducing squeal by modifying the contact block of the brake pad[3] and proposes a method to reduce squeal using the squeal sensitivity of contact stiffness. Note that the test body

used in the present study is a floating type front-wheel disk brake for a passenger vehicle. In addition, in order to prevent the analysis results from being overly complex, the target frequency is set to 10 kHz, and the vibration mode of the rotor is limited to the diameter node type.

2. Measuring the Load Distribution on a Contact Surface

2. 1 Original Sensor and Measurement Conditions

Figure 1 shows the structure of the developed sensor. This sensor incorporates a friction sensor and a load detection sensor. The load detection sensor is a parallel flat board-type sensor.[11] When a friction force acts on the sensor, the strain on the end of the flat board increases. Therefore, four strain gages, which are positioned as shown in the figure, detect the friction force. The generated strain ε, which is given below, consists of the first term of the shearing element and the second term of the bending element:

$$\varepsilon = \frac{F_S}{Ebt}\left(\frac{3l}{2t} + \frac{l+l'}{h}\right) , \qquad (1)$$

where E is Young's modulus, b is the depth of the sensor, t is the thickness of the parallel board, h is the width of the opening, Fs is the shear force, l is the length of the opening, and l' is the distance from the end of opening to the end of the sensor.

The other strain gages, which are placed at the center of flat boards, detect the compression load and measure the force normal to the rotor. Two friction surface portions of the sensor are removed from a practical rotor and processed into cylindrical form and then fixed to the load detection sensor by press-fitting.
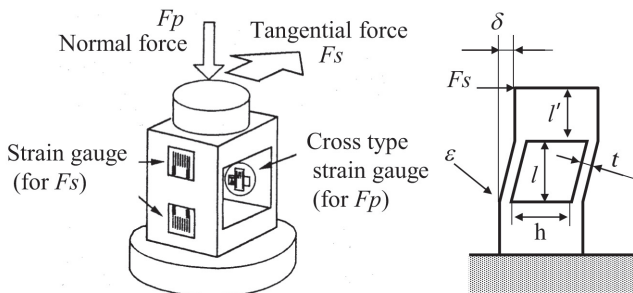
The typical design size of a sensor in this study is a friction sensor with a sensing surface portion that is 5 mm in diameter and an opposite surface portion that is 14 mm in diameter. The fixed friction sensor used in the experiment is press-fit into a rotor, as shown in **Fig. 2**. The inner and outer sensors of the rotor are placed so as to operate in opposite directions. The placements of sensors in an array are determined by both the sensor size and the location of ventilated fins.

2. 2 Application Examples for the Developed Sensor

2. 2. 1 Influence of Caliper Alignment

The relative positional relation between a rotor and a caliper sometimes changes,[12] for example, when a lateral force acts on the tires of a turning vehicle. This section investigates the influence of caliper alignment on the load distribution. **Figure 3** shows the drag-type test rig used in the squeal experiment. The target is a floating-type disk brake commonly used in passenger
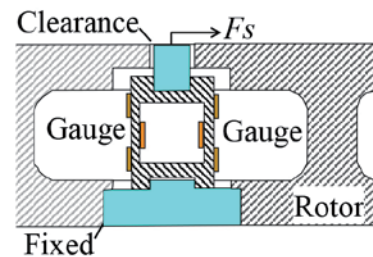
Fig. 2　Sensor built into rotor.

Reprinted from Transactions of JSAE, Vol. 41, No. 2 (2010), pp. 207-212, © 2010 JSAE.

Fig. 1　Sensor structure.

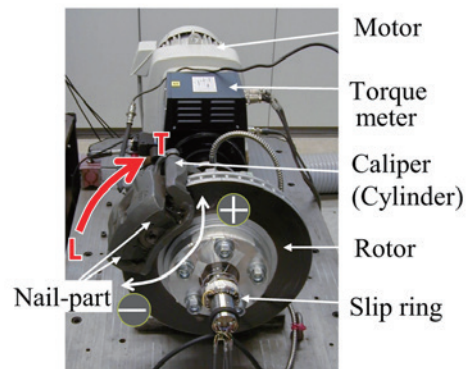Reprinted from Transactions of JSAE, Vol. 41, No. 2 (2010), pp. 207-212, © 2010 JSAE.

Fig. 3　Drag test rig.

Modified from Transactions of JSAE, Vol. 41, No. 2 (2010), pp. 207-212, © 2010 JSAE.

vehicles. The components for changing the caliper alignment are attached to the bolt tightening assembly of a mounting bracket. These special components for changing caliper alignment allow the relative angle between the pads and a rotor to be varied from +1 degree to –1 degree.

The sensors pass through the center of the pad in the radial direction of the pad. The phase between the two sensors is set to be 180 degrees. One sensor is for measuring the inner pad, whereas the other is for the outer pad. **Figure 4** shows the load distribution for a standard alignment. The temperature of the rotor surface is 60°C. The upper and lower figures show the results for the inner and outer pads, respectively. The normal force and the friction force are shown for various braking torques. The horizontal axis of the graph shows the rotation angle of the rotor, which corresponds to the sensor position in the circumferential direction of the pad. The friction coefficient μ is obtained as the ratio of the normal force to the friction force. In this case, μ is estimated to be 0.4, except at two points, namely, at approximately 15 degrees and at approximately 35 degrees, at which μ decreases. These locations correspond to the positions of holes in the backing plate. These decreases in μ are considered to be due to the manufacturing of the pad, which is made to be thin in these locations.
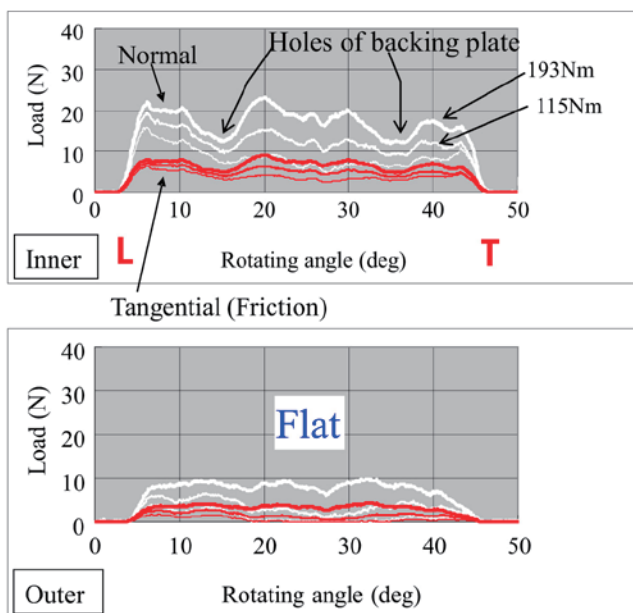
Figure 5 shows the load distributions for a caliper alignment of +1 degree. The load distribution of the outer pad is inclined toward the trailing side (hereinafter, T side). This is due to the caliper alignment, that is to say, the "nail" part of the cylinder located at the T side strongly compresses the backing plate of the pad. The amplitude of the squeal noise becomes high in the braking torque range of from 140 to 180 Nm.

2. 2. 2 Influence of the Temperature of the Frictional Material

The relationship between the rotor temperature and the load distribution is investigated for the previously described brake. The results of the investigation are shown in **Figs. 6** and **7**. When the rotor temperature is 20°C, both the inner and outer pads have large loads at the leading side (hereinafter, L side) and at the T side. When the rotor temperature reaches 100°C, the outer pad has a trapezoidal load distribution, and the inner pad has triangular load distribution. The apex of the triangular distribution moves from the L side toward the center of the pad. This difference in the load distribution between the inner and outer pads depends on the press components, such as the nail part and the piston of the brake caliper. Squeal readily occurs when the temperature of the rotor is 20°C and
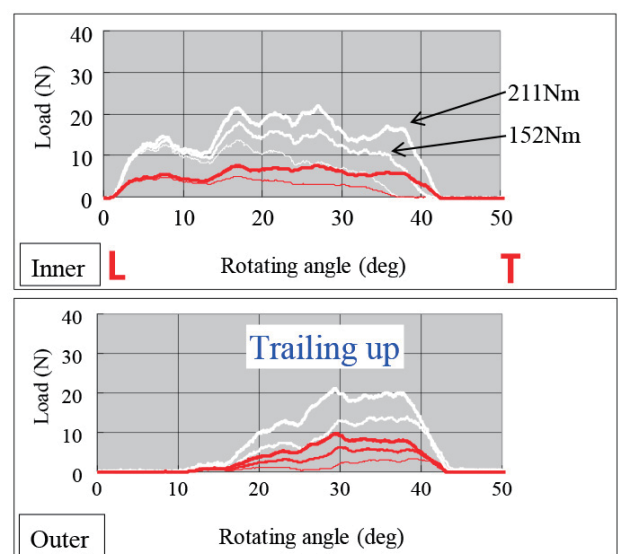

Fig. 4   Load distributions (Angle: 0, Temp.: 60°C).
Reprinted from Transactions of JSAE, Vol. 41, No. 2 (2010), pp. 207-212, © 2010 JSAE.

Fig. 5   Load distributions (Angle: +1 degree, Temp.: 60°C).
Reprinted from Transactions of JSAE, Vol. 41, No. 2 (2010), pp. 207-212, © 2010 JSAE.

the braking torque is set to be within the range of from 80 to 180 Nm. In this way, the load distribution on the friction surface is demonstrated to be affected by the rotor temperature, and deviation of the load on the L or T side causes squeal.

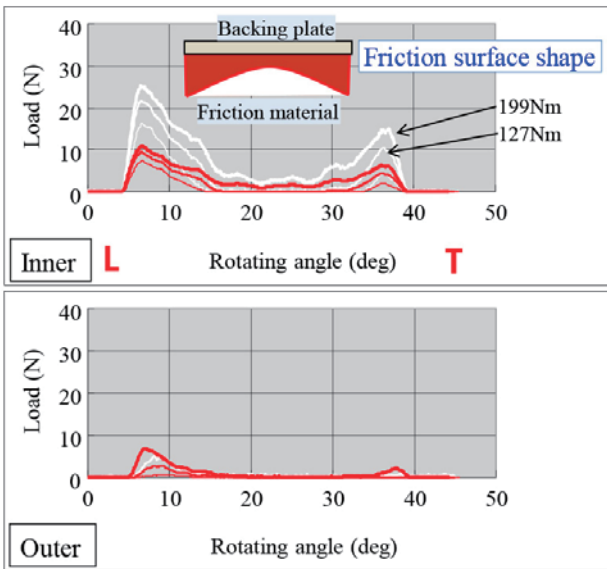In the case of a relatively lower temperature of the

Fig. 6　Load distributions (Temp.: 20°C).

Modified from Transactions of JSAE, Vol. 41, No. 2 (2010), pp. 207-212, © 2010 JSAE.
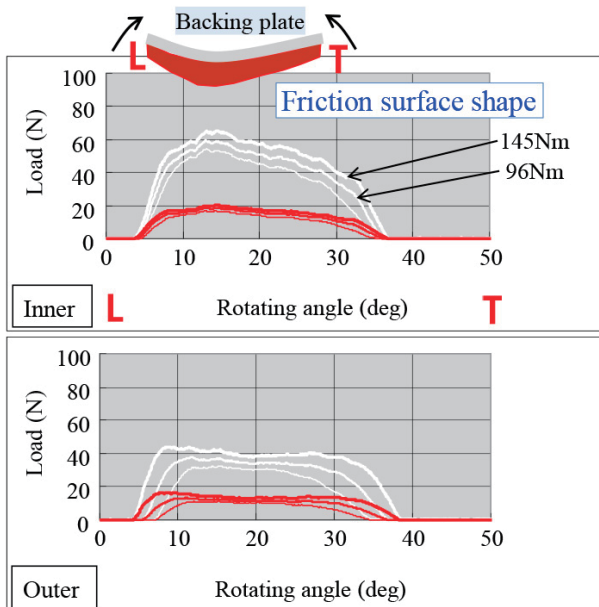

Fig. 7　Load distributions (Temp.: 100°C).

Modified from Transactions of JSAE, Vol. 41, No. 2 (2010), pp. 207-212, © 2010 JSAE.

rotor, the loads in the circumferential direction at both ends of the pad become large, primarily as a result of thermal deformation. The friction material of the pad includes a great deal of resin, the coefficient of thermal expansion of which is larger than that of the metal of the backing plate. Therefore, both ends of the pad warp toward the backing plate when the temperature increases. In contrast, both ends of the pad warping toward the rotor when the temperature decreases. In this experiment, facing up condition is conducted at a controlled temperature of from 60°C to 80°C. Therefore, the load distribution of the pad is basically flat for a constant-temperature condition. When the temperature becomes lower than the facing up condition, both ends of the pad warp toward the rotor and receive an increased load. When the temperature exceeds the facing up condition, the center position of the pad is warp toward the rotor and receives increased load around the center of the friction area.

In order to further investigate the relationship between temperature and load distribution, an experiment is conducted using the equipment shown in **Fig. 8**. The inertial mass of this instrument is equivalent to that of a vehicle. Therefore, the experiment can be performed under actual braking conditions. A floating-type disk brake is newly adopted as a specimen for the experiment. The braking time is 5 seconds, and the idling time is 10 seconds. The experiment alternates between
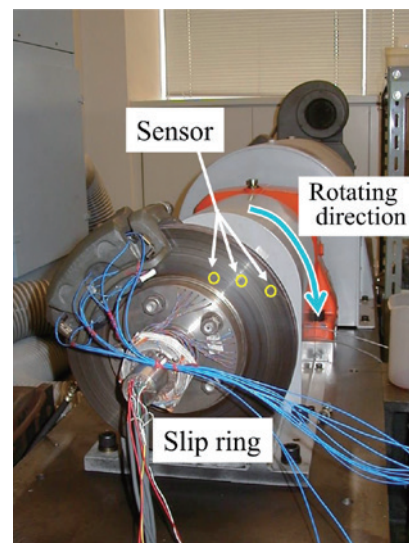

Fig. 8　Test rig with vehicle inertia.

Modified from Transactions of JSAE, Vol. 41, No. 2 (2010), pp. 207-212, © 2010 JSAE.

braking and idling until the temperature of the outer peripheral end of the rotor reaches 200°C. The rotor speeds at the start of braking are set to 171 rpm (vehicle speed: 20 km/h) and 428 rpm (vehicle speed: 50 km/h). Brake fluid pressures of 0.5, 1.0, and 1.5 MPa are considered. The temperature and friction force distributions for the outer pad are measured while increasing the temperature. Temperature is measured at nine points within the friction material area and at two points within the backing plate, as shown in **Fig. 9**. Figure 8 shows three measurement points on the rotor: one toward the inner circumference of the rotor, one toward the outer circumference of the rotor, and one in the center of the rotor. The points are separated circumferentially by 13.85 degrees.

Figure 10 shows the results for the case in which the measurement temperature increases uniformly as the number of braking cycles increases. In this experiment, the vehicle speed is 50 km/h, and the brake fluid pressure is 1 MPa. Comparing the results in the radial direction, the outer temperature is higher than the inner temperature. The temperature of the middle area in the radial direction indicates that, if anything, the intermediate value between the inner periphery side and the outer periphery side is closer to the temperature of the outer periphery side. The difference in temperature in the circumferential direction is not greater than that in the radial direction. Sometimes the temperature of central area of the pad becomes high, but on the whole, the temperature of
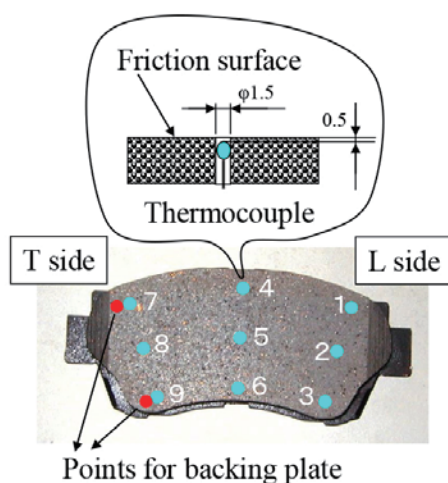
the T side is inclined to be higher than that of the L side. For example, when the number of braking cycles is 21, the difference in temperature between the inner periphery side and outer periphery side is 45°C. On the other hand, the difference in temperature between the outer side and the backing plate is 132°C. Thus, the temperature varies in the circumferential direction and in the radial direction as well as between the friction material and the backing plate. Therefore, the pad undergoes thermal deformation, which affects the distribution of the friction force.

Figure 11 shows the results of the distribution of the friction force under the braking condition, where the vehicle speed is 20 km/h and the brake fluid pressure is 1.5 MPa. The upper graph shows the friction force at 50°C with respect to the rotor temperature, and the lower graph shows the friction force at 200°C with respect to the rotor temperature. The horizontal axis represents the braking duration. Because of the sensor insertion points, the three sensor signals exhibit some phase difference. The figure shows, from left to right, the outer point, the middle point, and the inner point. At a temperature of 50°C, the friction force of the T side becomes large, and the friction force of the inner point becomes large over a wide circumferential area. At a temperature of 200°C, the friction forces of the L side and the T side become small, and the friction force of the entire area becomes large. In particular, the friction force of the outer periphery becomes larger than that of the inner periphery. Thus, the
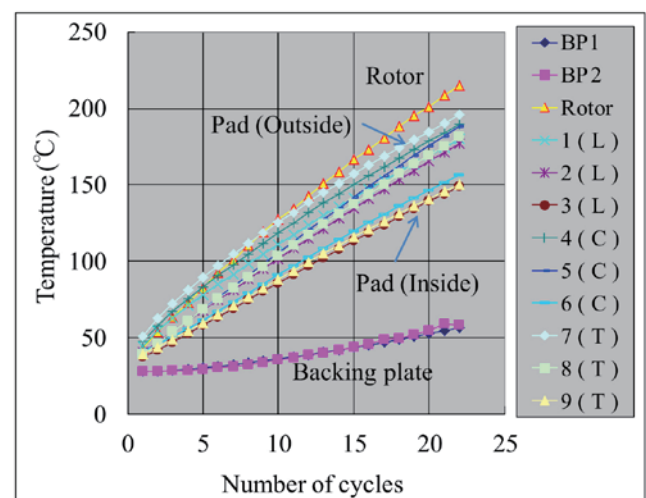

Fig. 9   Measuring points of pad temperature.
Reprinted from Transactions of JSAE, Vol. 41, No. 2 (2010), pp. 207-212, © 2010 JSAE.

Fig. 10   Temperature by repeated brake operations.
Reprinted from Transactions of JSAE, Vol. 41, No. 2 (2010), pp. 207-212, © 2010 JSAE.

distribution of the pad temperature changes according to the rotor temperature, and the pad exhibits thermal deformation, as a result of the change in the friction force distribution, which affects brake squeal.

3. Method for Calculating Squeal Reduction

3. 1 Outline of the Calculation Method

Figure 12 shows the calculation flow. First, mode reduction is applied to each target component, such as

Fig. 11   Load distributions at 3 changed radius points.

Modified from Transactions of JSAE, Vol. 41, No. 2 (2010), pp. 207-212, © 2010 JSAE.

Fig. 12   Calculation flow of squeal analysis.

Reprinted with permission from SAE Tech. Paper Ser., No. 2010-01-1691, © 2010 SAE International.

the brakes, in order to express the part characteristics as eigenvalues. Each joint between a pair of contact points is modeled as a spring of equivalent stiffness. Appropriate values are used for the spring constants of the contact portions with respect to brake fluid pressure and frequency.[13] In addition, for areas of contact that experience friction, such as that between the rotor and the pad, a friction coefficient is also set. A characteristic equation of the brake assembly is then created based on these properties in order to enable complex eigenvalue analysis. The susceptibility to squeal (degree of divergence) can be obtained from the real part of the complex eigenvalues, and the squeal frequency can be obtained from the imaginary part of the complex eigenvalues. The normalized value for achieving the target damping coefficient rate of 1 is used for the squeal index.

Since a squeal calculation method using mode reduction has already been reported,[14] the present article focuses on a method for reducing squeal, with a brief explanation of mode reduction. **Figure 13** shows a vibration system composed of two substructures, labeled 1 and 2, which are connected by springs at connecting region '*b*'. Here, '*a*' denotes the internal region of each substructure. The equation of motion can be expressed as follows:
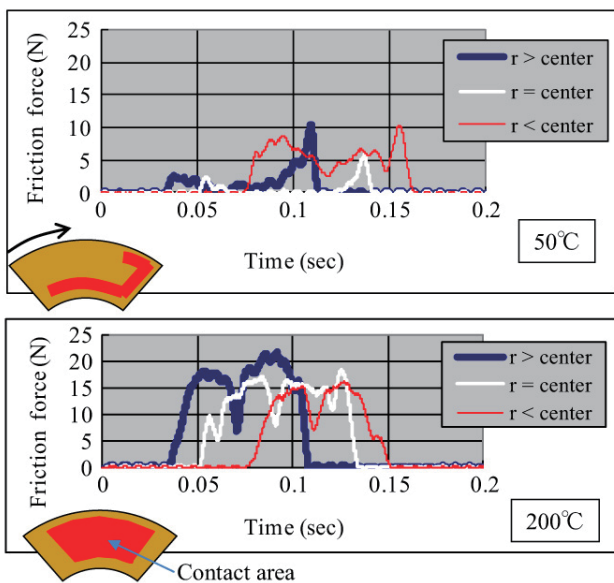
$$
\begin{bmatrix}
M_{aa}^{(1)} & M_{ab}^{(1)} & 0 & 0 \\
M_{ba}^{(1)} & M_{bb}^{(1)} & 0 & 0 \\
0 & 0 & M_{aa}^{(2)} & M_{ab}^{(2)} \\
0 & 0 & M_{ba}^{(2)} & M_{bb}^{(2)}
\end{bmatrix}
\begin{Bmatrix}
\ddot{x}_a^{(1)} \\
\ddot{x}_b^{(1)} \\
\ddot{x}_a^{(2)} \\
\ddot{x}_b^{(2)}
\end{Bmatrix}
$$

$$
+
\begin{bmatrix}
K_{aa}^{(1)} & K_{ab}^{(1)} & 0 & 0 \\
K_{ba}^{(1)} & K_{bb}^{(1)}+K_{c11} & 0 & K_{c12} \\
0 & 0 & K_{aa}^{(2)} & K_{ab}^{(2)} \\
0 & K_{c21} & K_{ba}^{(2)} & K_{bb}^{(2)}+K_{c22}
\end{bmatrix}
\begin{Bmatrix}
x_a^{(1)} \\
x_b^{(1)} \\
x_a^{(2)} \\
x_b^{(2)}
\end{Bmatrix}
=
\begin{Bmatrix}
f_a^{(1)} \\
0 \\
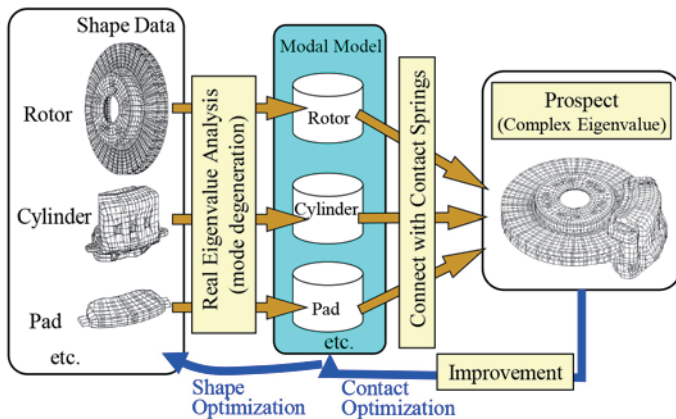f_a^{(2)} \\
0
\end{Bmatrix}, \quad (2)
$$

where

$\{x\} = \left\{ x_a^{(1)} \ x_b^{(1)} \ x_a^{(2)} \ x_b^{(2)} \right\}^T$: the response vector

$\{f\} = \left\{ f_a^{(1)} \ 0 \ f_a^{(2)} \ 0 \right\}^T$: the force vector

$[M_{jk}^{(l)}]$: the mass matrices of substructures, (l = 1, 2), (j = a, b), (k = a, b)

$[K_{jk}^{(l)}]$: the stiffness matrices of substructures, (l = 1, 2), (j = a, b), (k = a, b)

$\begin{bmatrix} K_{c11} & K_{c12} \\ K_{c21} & K_{c22} \end{bmatrix}$: the stiffness matrices composed of connecting springs, referring to Eq. (3)

$$\begin{bmatrix} K_{c11} & K_{c12} \\ K_{c21} & K_{c22} \end{bmatrix} = \begin{bmatrix} \mu k_i & -\mu k_i \\ k_i & -k_i \\ -\mu k_i & \mu k_i \\ -k_i & k_i \end{bmatrix}. \tag{3}$$

If the constrained mode synthesis method is applied to Eq. (2), the spatial coordinates $\{x\}$ are transformed to the new coordinates $\{z\} = \{x_b^{(1)} \quad x_b^{(2)} \quad \xi^{(1)} \quad \xi^{(2)}\}^T$, which consist of modal coordinates and connecting points. The transformed matrices are as follows:

$$\begin{Bmatrix} x_a^{(1)} \\ x_b^{(1)} \\ x_a^{(2)} \\ x_b^{(2)} \end{Bmatrix} = \begin{bmatrix} \phi_b^{(1)} & T^{(1)} & 0 & 0 \\ 0 & I & 0 & 0 \\ 0 & 0 & \phi_b^{(2)} & T^{(2)} \\ 0 & 0 & 0 & I \end{bmatrix} \begin{Bmatrix} \xi^{(1)} \\ x_b^{(1)} \\ \xi^{(2)} \\ x_b^{(2)} \end{Bmatrix} = T \begin{Bmatrix} \xi^{(1)} \\ x_b^{(1)} \\ \xi^{(2)} \\ x_b^{(2)} \end{Bmatrix} \tag{4}$$

where

$\phi_b^{(i)}$: the constrained mode vector of substructure i, $(i = 1, 2)$

$\xi^{(i)}$: the modal coordinates of substructure i, $(i = 1, 2)$

I : the identity matrix

T : the transfer matrix

$$\left[T^{(i)}\right] = -\left[K_{aa}^{(i)}\right]^{-1}\left[K_{ab}^{(i)}\right], (i = 1, 2). \tag{5}$$

The following is obtained by substituting Eq. (4) into Eq. (2), and left-multiplying by T^T:

$$T^T M\, T \begin{Bmatrix} \ddot{\xi}^{(1)} \\ \ddot{x}_b^{(1)} \\ \ddot{\xi}^{(2)} \\ \ddot{x}_b^{(2)} \end{Bmatrix} + T^T K\, T \begin{Bmatrix} \xi^{(1)} \\ x_b^{(1)} \\ \xi^{(2)} \\ x_b^{(2)} \end{Bmatrix} = T^T \{f\}. \tag{6}$$

If the modal mass $\overline{M}$ and the modal stiffness $\overline{K}$ are adopted, and the external forces are free, Eq. (6) is rewritten as follows:

$$\overline{M}\ddot{z} + \overline{K}z = 0. \tag{7}$$
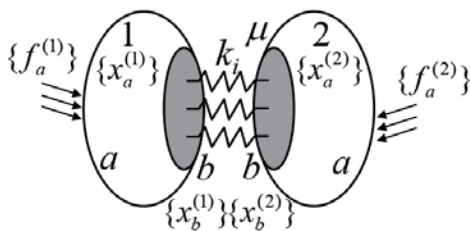
Fig. 13 Vibration system composed of two substructures.

Figure 14 shows the stiffness matrix of Eq. (7) in pattern form, which consists of the eigenvalues for each substructure, the joint contact stiffness, and μ. Accordingly, when studying squeal reduction, it is possible to fix the part eigenvalues and use the contact stiffness as a design variable, or conversely, to fix the contact stiffness of the joints and use the part eigenvalues as the design variable.

3. 2 Squeal Simulation Using Contact Blocks

There are many cases of contact between two parts in a disk brake. These include contact between the pad friction material and the rotor, contact between the backing plate of the pad (torque support abutment) and the mount bracket (hereinafter, mount), contact between the backing plate of the pad and the finger of the brake cylinder, and contact between the backing plate of the pad and the piston. (In the last two cases, a shim is usually interposed between the parts.) We herein analyze the design between the pad and the rotor, because these contact portions are more susceptible to squeal.

As shown in **Fig. 15**, the contact area of the pad is divided into eight blocks, labeled A through H. Various combinations are considered in order to investigate the contact conditions that are capable of reducing squeal. A total of 57 squeal calculations are performed, where the conditions are varied from the conditions in which each of the blocks, from A to H, is set to be in the
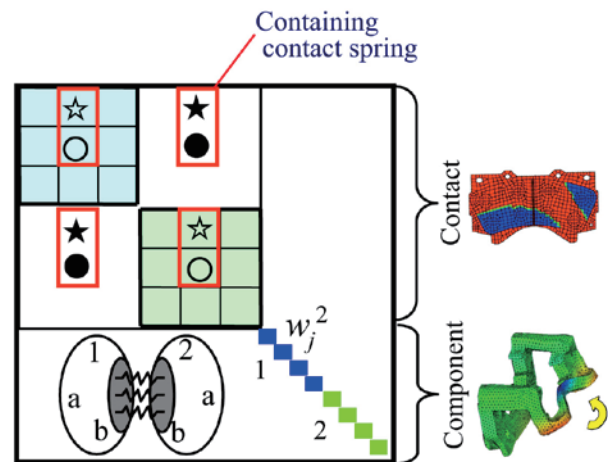

Fig. 14 Outline of stiffness matrix composed of body 1 and body 2.

non-contact condition to the condition in which a maximum of six blocks are set to be in the non-contact condition. The analysis conditions for the non-contact blocks also included setting the inner and outer pads to the same position and setting the inner and outer contact positions to mutually different points. The stability calculation for the squeal requires a complex eigenvalue analysis with a constant friction coefficient.

Figures 16 and **17** show the results of the stability calculation as the contact position between the rotor and the pad is varied. The vertical axis shows the complex eigenvalue of the real part as a squeal susceptibility index. The horizontal axis shows the squeal frequency obtained from the imaginary part. Parallel shifts in the depth direction indicate the state of squeal with respect to each condition when the contact position is varied. The front-most results in each figure are the results for the case in which the entire surface of the rotor and the pad are in contact and can be used as a reference.

The calculation results indicate that if the L side or the T side is set to the non-contact condition, then low-frequency (1.6 kHz) squeal can be reduced. These results are consistent with the results obtained from the experiment described in Section 2. However, squeal occurs at another frequency (3.4 kHz). Consequently, the method of combining contact blocks cannot stop squeal. When these types of brakes are operated, the squeal at a certain frequency can often be reduced, whereas that at other frequencies becomes worse. Thus, a design method that considers the contact region, which is effective for reducing squeal at multiple frequencies, is proposed in the following section.
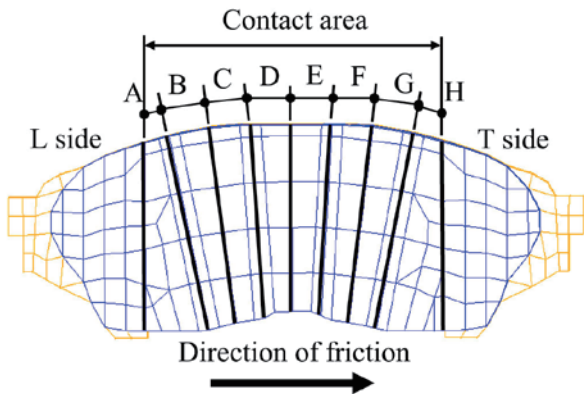
3. 3 Squeal Reduction through Sensitivity Analysis

3. 3. 1 Calculation Method

The equation of motion of a damped system can be expressed as follows:

$$M\ddot{u}(t) + C\dot{u}(t) + Ku(t) = f(t) , \qquad (8)$$

where M, C, and K are the matrices of mass, damping, and stiffness, respectively, f is the excitation force vector, and u is the response displacement vector. If y is defined as the differential of u, then the following equation is obtained:

$$y(t) = \dot{u}(t) . \qquad (9)$$

Fig. 16 Squeal map (the number of contact = 6, facing).
Reprinted with permission from SAE Tech. Paper Ser., No. 2010-01-1691, © 2010 SAE International.

Fig. 15 FE model of a pad which is divided into 8 blocks.
Reprinted with permission from SAE Tech. Paper Ser., No. 2010-01-1691, © 2010 SAE International.
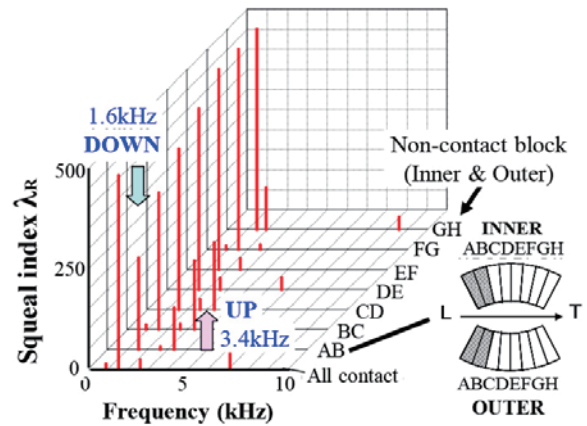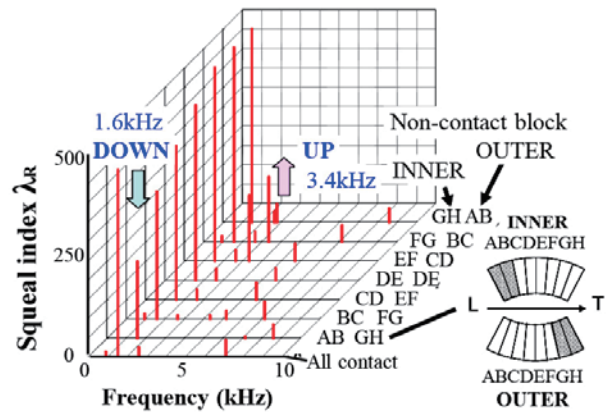

Fig. 17 Squeal map (the number of contact = 6, not facing).
Reprinted with permission from SAE Tech. Paper Ser., No. 2010-01-1691, © 2010 SAE International.

Substituting Eq. (9) into Eq. (8) and rearranging yields the following:

$$M\ddot{u}(t) - M\ddot{u}(t) = M\dot{u}(t) - M\,y(t) = 0 \tag{10}$$

$$C\dot{u}(t) + M\dot{y}(t) + Ku(t) + \begin{bmatrix} 0 \end{bmatrix} y(t) = f(t)$$
$$M\dot{u}(t) + \begin{bmatrix} 0 \end{bmatrix}\dot{y}(t) + \begin{bmatrix} 0 \end{bmatrix} u(t) - M\,y(t) = 0 \tag{11}$$

$$\begin{bmatrix} C & M \\ M & 0 \end{bmatrix}\begin{Bmatrix} \dot{u} \\ \dot{y} \end{Bmatrix} + \begin{bmatrix} K & 0 \\ 0 & -M \end{bmatrix}\begin{Bmatrix} u \\ y \end{Bmatrix} = \begin{Bmatrix} f \\ 0 \end{Bmatrix}\ , \tag{12}$$

where

$$A = \begin{bmatrix} K & 0 \\ 0 & -M \end{bmatrix}, B = \begin{bmatrix} C & M \\ M & 0 \end{bmatrix}, \text{ and } w = \begin{Bmatrix} u \\ y \end{Bmatrix}\ . \tag{13}$$

The solution of the free vibration of Eq. (12) can be assumed as follows:

$$w(t) = we^{\lambda t}\ . \tag{14}$$

Then, Eq. (11) is written as

$$B\dot{w} + Aw = 0\ , \tag{15}$$

which can be conveniently rewritten as follows:

$$Aw + \lambda Bw = 0 \tag{16}$$

$$v^T A + \lambda v^T B = 0\ , \tag{17}$$

where

λ : the eigenvalue
w : the right eigenvector
v : the left eigenvector .

The following equation is used to calculate the squeal sensitivity for each stiffness element k_i :

$$\frac{\partial \lambda}{\partial k_i} = -\ \frac{v^T (\frac{\partial A}{\partial k_i} + \lambda \frac{\partial B}{\partial k_i})w}{v^T B\ w}\ . \tag{18}$$

Note that Eq. (18) is established in the same manner upon mode reduction. Eq. (18) is used to calculate the squeal sensitivity of the springs distributed at the target contact portions. In the sensitivity calculation, partial differentiation is applied to the items related to the target springs in the stiffness matrix. This squeal reduction method involves removing various combinations of high-sensitivity springs and is referred to as the high-sensitivity spring component removal method. Here, in order to perform the calculation efficiently, at the stage where the physical degree of freedom can be obtained explicitly, partial differentiation is applied to the μk_i and k_i elements related to contact stiffness with respect to k. Conversion to mode coordinates is performed after replacing them with μ and 1. Items requiring conversion to mode coordinates include

eight items on the friction surface and four non-friction surface items. This method can reduce the matrix scale and greatly shorten the calculation time.

3. 3. 2 Application Cases

Figures 18 and **19** show the sensitivity calculation for the cases using a 14-inch ventilated rotor. The left-hand side of the figures shows the data for outer pad and the right-hand side shows the data for the inner pad. The L side is at the top, and the T side is at the bottom. The length of the line extending from each node expresses the squeal sensitivity, and the orientation of the line indicates whether the sensitivity is positive or negative. Lines extending outward from the paper are positive, and lines extending into the paper are negative. Positive squeal sensitivity means
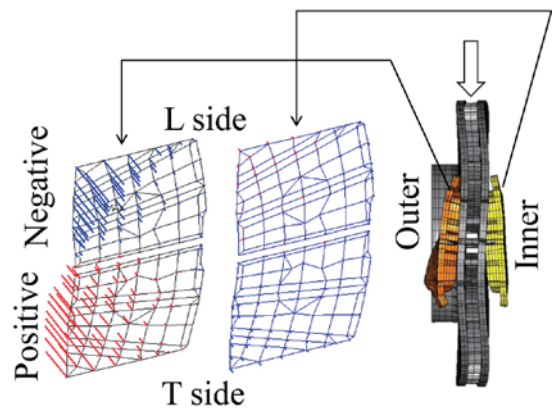

Fig. 18   Sensitivity of contact spring (4600 Hz, brake B).
Reprinted with permission from SAE Tech. Paper Ser., No. 2010-01-1691, © 2010 SAE International.
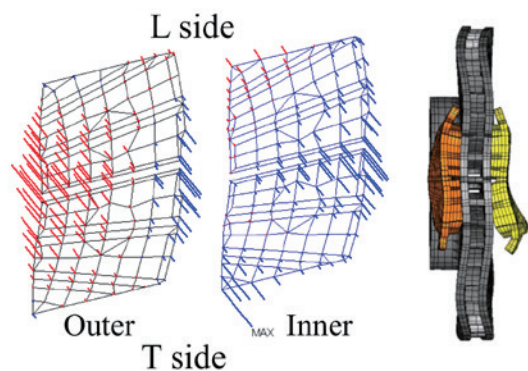

Fig. 19   Sensitivity of contact spring (7876 Hz, brake B).
Reprinted with permission from SAE Tech. Paper Ser., No. 2010-01-1691, © 2010 SAE International.

that increasing stiffness would increase the squeal susceptibility.

Table 1 lists the results of the squeal analysis. This table lists the results for three brakes: a brake with a smaller diameter rotor than that described above A, the brake described above B, and a brake with a larger diameter rotor than that described above C. The inner pad of brake A tends to have a high sensitivity, and the portions of high sensitivity change depending on the frequency. The L sides of both the inner and outer pads of brake C have high sensitivity. As such, the squeal sensitivity of springs located between parts varies. However, since the squeal sensitivity depends on the vibration mode, the region with the same polarity expands at comparatively low frequencies, where the rotor and pad form low-order vibration modes. In contrast, the polarity tends to move in a complex manner within a narrow area in high-frequency regions.

Since the overall squeal sensitivity of the pad on the L side of brake C is high, chamfering is applied to both end surfaces in order to provide a common shape for the inner and outer pads in consideration of cost. **Figure 20** shows the obtained results. Without chamfering, 6- to 8-kHz squeal occurs, as indicated by the red data points labeled 5ND, 6ND, and 7ND. The 6- to 8-kHz squeal is eliminated by the chamfering.

In the case described above, the sensitivity trend is relatively uniform. However, when the sensitivity changes in a complex manner, optimization must be achieved in several steps in order to gradually remove

areas of high sensitivity. **Figures 21**(a) and (b) show the data for a case in which high-frequency squeal between 5 and 10 kHz is reduced to zero in the sixth optimization step. In this case, as shown in **Fig. 22**, there are only a few non-contact areas. **Figure 23** shows the friction surface, which is calculated to reduce the squeal around 2 kHz. For squeal reduction, it is
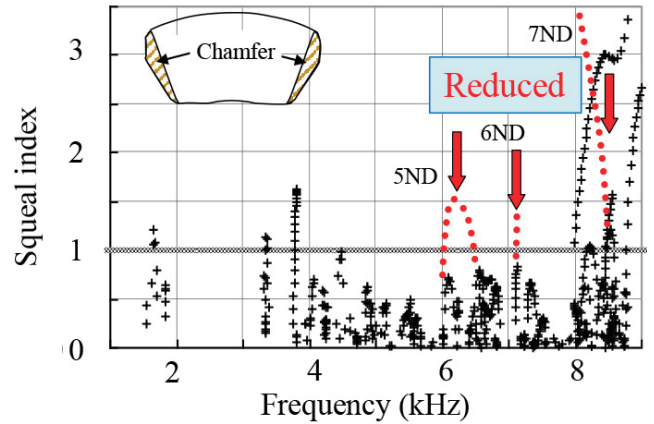

Fig. 20 Chamfer effect displayed in squeal map (brake C).

Reprinted with permission from SAE Tech. Paper Ser., No. 2010-01-1691, © 2010 SAE International.

Table 1 Results of sensitivity analysis.

Brake	Freq. (Hz)	Pressure (3 level)	High Sensitive of Outer Pad	High Sensitive of Inner Pad
A	5167	Low	In(−), Out_L(+)	Out_L(+)
	6741	Low	---	In_L(−)_T(+)
	8145	Middle	---	In_T(−)
	9207	Middle	---	In_L(+)_T(+)
B	4600	Low	In_L(−)_T(+)	---
	7876	Middle	In_Center(+)	Out_Cen (−), In_T(−)
	8130	Middle	---	Out_T(+)
C	3653	Low	In&Out_L(−)	In&Out_L(+)
	6337	Middle	In&Out_L(+)	---
	7146	High	---	In&Out_L(+)
	7985	High	---	In&Out_L(+)

Reprinted with permission from SAE Tech. Paper Ser., No. 2010-01-1691, © 2010 SAE International.
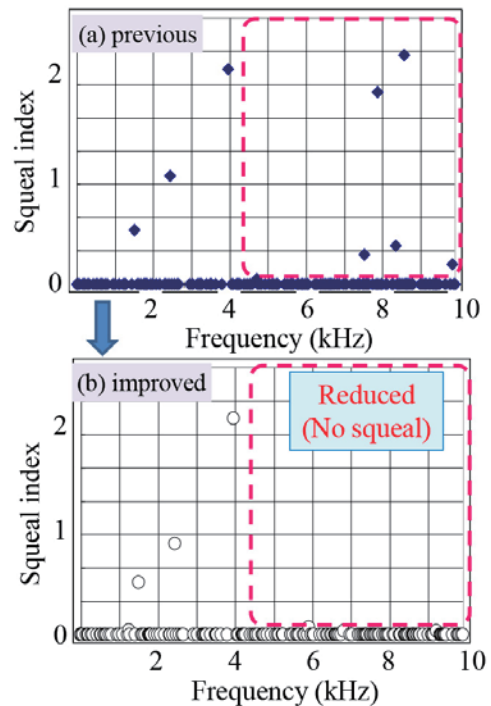

Fig. 21 Example of squeal reduction.

Reprinted with permission from SAE Tech. Paper Ser., No. 2010-01-1691, © 2010 SAE International.

necessary to prevent contact over large areas of both the inner periphery of the L side and the outer periphery of the T side. Since it is not practically possible to substantially decrease the size of the friction surface, it is not appropriate to use contact optimization as a countermeasure to reduce low-frequency squeal. Since component parts form low-order vibration modes at low frequencies, it is preferable to reduce squeal by modifying the design of the parts.

4. Summary

The contact condition of the friction surface has a significant influence on brake squeal. Therefore, the present study examined technology for measuring
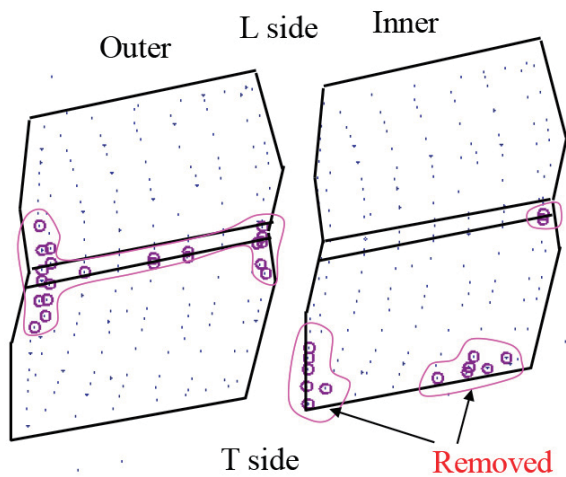

Fig. 22 Removed area for high frequency squeal (Optimized small chamfer).

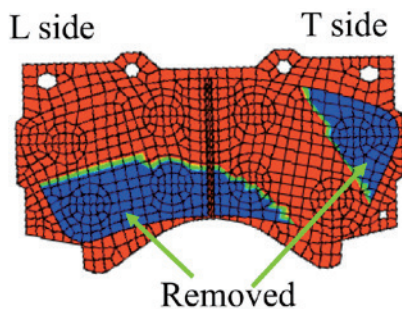Reprinted with permission from SAE Tech. Paper Ser., No. 2010-01-1691, © 2010 SAE International.

Fig. 23 Example of removed area for about 2 kHz squeal (Large chamfer is needed for low frequency).

Reprinted with permission from SAE Tech. Paper Ser., No. 2010-01-1691, © 2010 SAE International.

the distribution of normal pressure and friction forces between a disk rotor and pads and for the purpose of optimizing contact surfaces through sensitivity analysis. These results are summarized as follows:

(1) A novel sensor, which can measure both normal pressure and friction force under the braking condition, has been developed. This sensor includes a friction there are only a few non-contact portions and a load detection there are only a few non-contact portions. The friction portions of the sensor are removed from a practical rotor, and the load detection sensor has a parallel flat board structure. The sensors were built into rotors at different circumferential and radial positions. A number of application examples depending on the caliper alignment and the rotor temperature were presented, and the load distribution under the braking condition was clarified to be complicated and the sensor was demonstrated to be useful in analyzing the contact condition.

(2) Brake squeal is likely to occur when the friction force at the ends of the pads becomes large. The squeal simulation revealed that if the non-contact area is set to the L side or the T side, low-frequency squeal can be reduced, whereas another squeal sometimes occurs. In order to prevent trial and error in design, a method for designing contact regions that are effective in reducing multiple frequencies of squeal has been developed. The squeal sensitivity distributed to each node was calculated, and the squeal was reduced by removing contact spring components with high sensitivity. This method is effective at any frequency, but leads to an increased chamfering area when the low-frequency squeal is targeted.

References

(1) Oura, Y., Kurita, Y. and Matsumura, Y., "Influence of Dynamic Stiffness Contact Region on Disk Brake Squeal", *Transactions of the Japan Society of Mechanical Engineers, Ser. C* (in Japanese), Vol. 73, No. 731 (2007), pp. 1985-1991.

(2) Nakatsuji, T., Oda, N., Okubo, K. and Fujii, T., "Effect of Friction Force Distribution on Exciting Force of Brake Noise for Motorcycle Disk Brake", *Transactions of the Japan Society of Mechanical Engineers, Ser. C* (in Japanese), Vol. 72, No. 721 (2006), pp. 3016-3021.

(3) Goto, Y., Sugiura, N., Chiku, K., Matsushima, T. and Hayakawa, K., "Fundamental Study on Contact Shape Optimization between Components for Brake Squeal Reduction", *Transactions of the Japan Society of*

Mechanical Engineers, Ser. C (in Japanese), Vol. 75, No. 751 (2009), pp. 532-540.

(4) "Pressure Measurement Film PRESCALE", <http://www.fujifilm.com/products/prescale/>, (accessed 2014-06-04).

(5) "Tekscan Pressure Sensors", < http://www.tekscan. com/pressureSensors>, (accessed 2014-06-04).

(6) Kurita, T. et al., "Friction Testing Machine", Unexamined Patent Pub., H6-94600 (in Japanese).

(7) Miyauchi, K. et al., "Friction Testing Machine for Friction Material of Drum Brake", Unexamined Patent Pub., H08-297084 (in Japanese).

(8) Nagasawa, Y., "Analysis of Brake Squeal", *R&D Review of Toyota CRDL* (in Japanese), Vol. 28, No. 1 (1993), pp. 43-51.

(9) Millner, N., "An Analysis of Disc Brake Squeal", *SAE Tech. Paper Ser.,* No. 780332 (1978).

(10) Zhang, L. et al., "Component Contribution and Eigenvalue Sensitivity Analysis for Brake Squeal", *21st Annual Brake Colloquium and Exhibition, SAE Tech. Paper Ser.,* No. 2003-01-3346 (2003).

(11) Hatamura, Y., Iino, K., Ono, K. and Takada, R., "A Trial on a 6-axis Force Sensor for Robots", *Transactions of the Japan Society of Mechanical Engineers, Ser. C* (in Japanese), Vol. 54, No. 497 (1988), pp. 241-246.

(12) Doi, O., Kumamoto, F. and Baba, H., "A study in Reduction of Brake Squeal (Second Report)", *Proc. of JSAE Spring Annual Congress* (in Japanese), No. 15-06 (2006), pp. 9-12.

(13) Goto, Y. et al., "Experimental Identification Method for Interface Contact Stiffness of FE Model for Brake Squeal", *Braking 2004: Vehicle Braking and Chassis Control* (2004), pp. 143-155, Wiley.

(14) Kaneda, T. and Ishihara, K., "Analysis of Disk Brake Squeal Using Substructure Synthesis Method: 1st Report, Analysis of Phenomenon and Development of Calculation Method", *Transactions of the Japan Society of Mechanical Engineers, Ser. C* (in Japanese), Vol. 70, No. 694 (2004), pp. 1602-1608.

Yoshitsugu Goto
  Research Fields:
    - Mechanical Analysis of Brake Squeal and Brake Friction
    - Co-creation for a New Value Creation
  Academic Degree: Dr.Eng.
  Academic Societies:
    - The Japan Society of Mechanical Engineers
    - Society of Automotive Engineers of Japan

Yuji Nagasawa
  Research Field:
    - Tribology and Mechanism Analysis of Mechanical Engineering
  Academic Society:
    - The Japan Society of Mechanical Engineers

Toru Matsushima*
  Research Fields:
    - Analysis of Brake Squeal Phenomenon
    - Design Method on Suppression of Brake Squeal
  Academic Societies:
    - Society of Automotive Engineers of Japan
    - The Japan Society of Mechanical Engineers
    - The Japan Society for Precision Engineering
  Award:
    - Takagi Awards of Japan Society for Precision Engineering, 2012

* TOYOTA MOTOR CORPORATION